The International Journal of Advanced Manufacturing Technology (2019) 103:1709–1719
https://doi.org/10.1007/s00170-019-03672-8

ORIGINAL ARTICLE

High-throughput microstructure printing technology using inflatable thin membrane with microchannel

Mitsutoshi Makihata[1] · **Albert P. Pisano**[2]

Received: 19 December 2018 / Accepted: 29 March 2019 / Published online: 10 April 2019

Abstract

Low-cost manufacturing technology for a micro-sized structure is receiving a lot of attention as human society is getting mixed with sensors and electronics. A template printing technology which forms micro-patterns by letting ink dried within a solvent permeable template is an attractive alternative of traditional costly micro-fabrication. However, low printing speed and lack of scalability have been recognized as a major drawback of this method. Here, we propose a novel printing machine using an inflatable polymer template. It is expected that thin membrane improves the printing speed due to its high permeation speed; however, the theoretical prediction and experimental proof of this approach has not been studied. A 450-μm thick membrane is fabricated by the casting polydimethylsiloxane (PDMS) on a silicon master mold, fixed to a printer head, and inflated to contact with substrate uniformly. The permeation mechanism is investigated by using both of the numerical simulation and experiments and discovers that the diffusion in thin membrane obeys an analytical solution for Fick's diffusion in steady state, while a conventional bulk template (10 mm) is in non-steady state. The printing system composed of pneumatic lines, a flash sintering unit, and a printer head holds the membrane is prototyped to ensure reproducibility of this novel method, five times faster printing speed compared to the ordinal method is confirmed.

Keywords Template printing · Micro-3D printing · Microfluidics · Soft lithography

1 Introduction

Nowadays, low-cost manufacturing technology of microstructures has been getting attention as a pathway to realize disposable sensor and electronics. A conventional microfabrication technology using photolithography, deposition, and etching technology targets a high-volume product and running cost of the manufacturing process prevent further cost reduction. Because of the recent trend which price and variety are matter, the direct patterning with printing technology has been studied widely as a promising alternative to the conventional manufacturing process [1, 2].

Major printing technology uses an ink to transfer material onto substrate using mechanical method such as physical contact [3, 4] and jet from nozzle [5–8]. Those methods are widely used due to its high throughput and a capability of additive manufacturing [4, 9]. On the other hand, micro-sized three-dimensional (3D) structures [6, 10] are used in various fields, such as bumps for wafer level packaging[11, 12] and microneedles [13, 14]. So, the capability for 3D microprinting is expected to have an additional impact on the low-cost manufacturing technology. However, the printing with ink is not suitable for this purpose, because the shape of ink while drying is governed by surface tension.

A template printing has been proposed using an elastomer with micro pattern contacting with target substrate to be printed on [15, 16]. This printing principle is using solvent permeation of a polymer material to generate ink flow into a channel (permeation pumping [17–19]) and let it dries. In contrast to droplet-based printers, this technology enables to control the shape of ink while it is drying, which means high aspect ratio printing is possible. However, the printing speed of these printing methods are generally slow due to small permeation of the template, and printing procedure is too complicated to achieve automated manufacturing.

✉ Mitsutoshi Makihata
makifata@gmail.com

[1] Department of Mechanical and Aerospace Engineering, University of California San Diego, 9500 Gilman drive, La Jolla, 92093, San Diego, CA, USA

[2] Jacobs School of Engineering, University of California San Diego, 9500 Gilman drive, La Jolla, 92093, San Diego, CA, USA

Here, we propose the novel design of template printing with an inflatable thin template (Fig. 1). It is envisioned that ultra-thin membrane instead of bulk template enables higher printing speed due to high permeation rate and larger printing area by using pneumatic action of the template. However, to our best knowledge, there is no report studying neither theoretical prediction between thickness and printing speed nor embodiment of inflatable template printer. So, the following section presents a re-investigation of the ordinal template printer to create a theoretical model which realizes an accurate prediction of the printing speed in various conditions. The experimental proof of this method is carried with a printer prototype which is designed to improve reproducibility of evaluation of printing speed. In Sections 3 and 4, the demonstration of printing and evaluation of printing speed are conducted, respectively.

2 Principle of template printing and analysis

2.1 Dynamics of inks in a permeable template

First, the re-investigation of printing speed with ordinal block template is carried to understand the solvent behavior in PDMS template. As illustrated in Fig. 2a, the template printing can be divided into three stages. First, a pure solvent is filled between a substrate and a template for initiating a continuous flow from an ink reservoir to microchannel by the permeation pumping. Then, ink is feed at the ink reservoir to alternate the pure solvent with an ink. As inks flow, the concentration of inks increases and solidarization of ink will start at the end of the channel, where the ink flow is zero at. Here, the substrate must be flat enough to prevent leakage of ink. This means that layer-by-layer printing is difficult without planarization step like the damascene process. In this paper, we will focus on single layer printing.

Figure 2 b are sequential photographs of printing of a silver nanoparticle ink. An alternation of a clear solvent with opaque ink, followed by solidification of ink started from the end of a channel can be seen. A dried pattern is observable by diffraction. As shown in the figure, the drying speed of ink is slower than ink filling. This is because the ink filling process is altering the pure solvent with ink while drying process needs to increase an ink concentration everywhere in the channel including an ink reservoir. On the other hand, the density of printing pattern strongly affect the printing speed as shown in Fig. 2c. As we discussed later, this slower printing speed can be explained by the saturated PDMS between channels which prevents two-dimensional diffusions of a solvent.

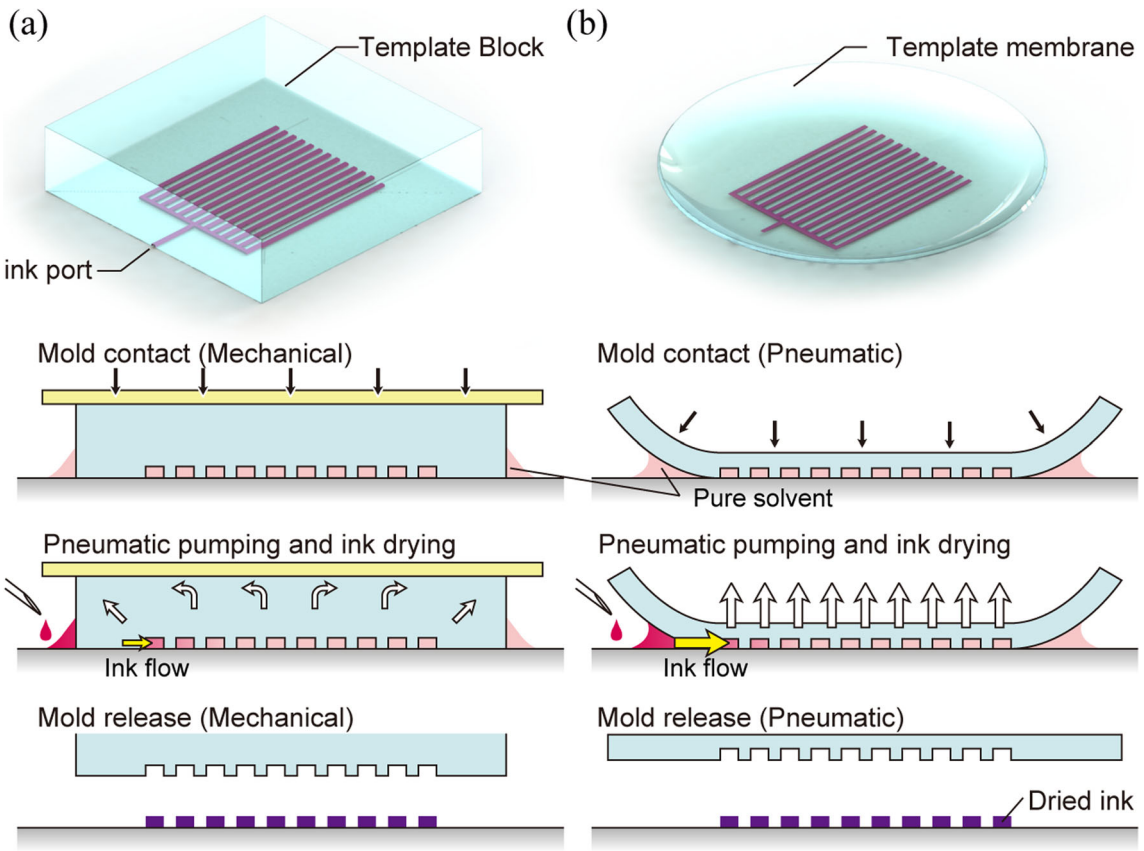

Fig. 1 Template printing **a** with ordinal block template **b** with membrane template

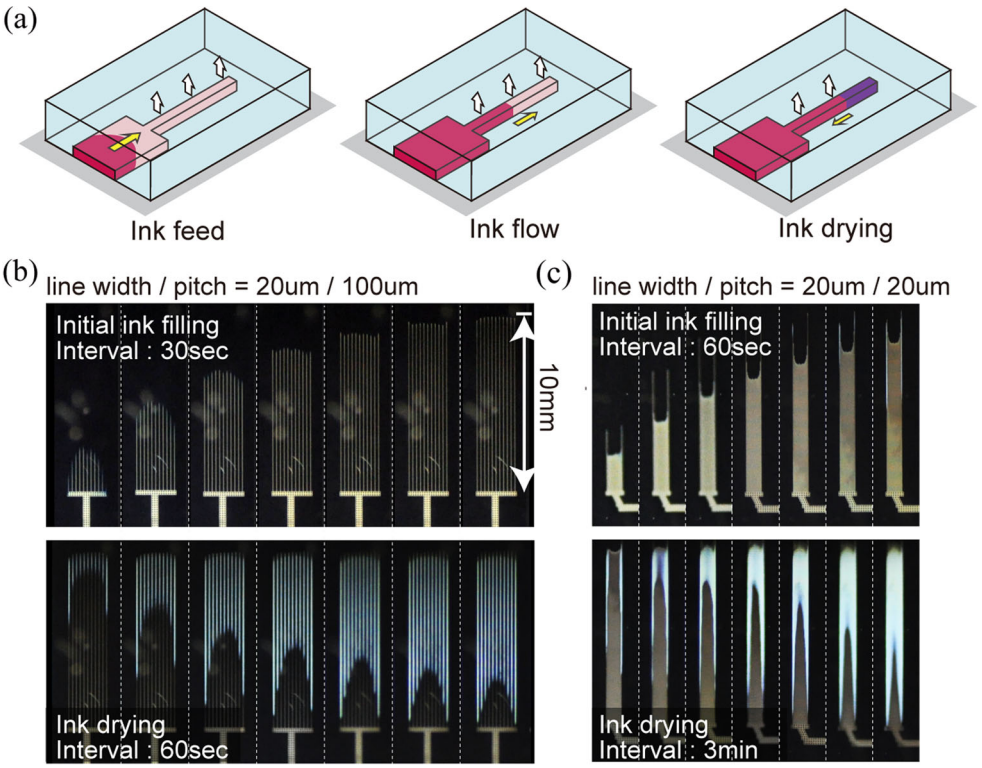

Fig. 2 Dynamics of ink in a solvent permeable template: **a** illustration of two printing stages, **b** snapshot of a silver ink filling and an ink drying stages of 20% density pattern, and **c** 50% pattern densities. Ten millimeter-thick PDMS (1:10 cured) block is used and printing temperature (T_P) is 43.3 °C

2.2 Permeation speed with diffusion analysis

The ink filling process is purely governed by the permeation and visually observable compared to the drying process. In this section, a permeation and printing speed are studied by comparing the computer simulation and experimental results. The ink filling process can be modeled by combining of a two-dimensional flux of solvent, $J_{2D}(\text{mol m}^{-1}s^{-1})$, and one-dimensional function of ink position $l(t)$ as shown in Fig. 3a, b [20]. Because only pure solvent area contributes ink flow, $l(t)$ satisfies following differential equation:

$$\frac{dl(t)}{dt} = -J_{2D}\frac{1}{A}\frac{M_i}{\rho_i}l(t), \tag{1}$$

where the A is cross-sectional area of the channel. The molar mass (M_i) and the density of solvent of ink (ρ_i) appears to convert the molar mass flux to volume change as time. In this study, ethanol (EtOH)-based ink is used. Here, the two-dimensional flux, J_{2D} can be classified into two cases: steady solution and non-steady solution. A flux at a boundary of steady state is constant with time, while the one for non-steady state decreases with time until it reaches the steady state.

Before moving to the calculation of J_{2D} using the finite element method (FEM) simulation, it is worth to introduce an analytical solution of one-dimensional Fick's diffusion equation to know the order of values and time dependency, also to verify the accuracy of FEM simulation. The diffusive

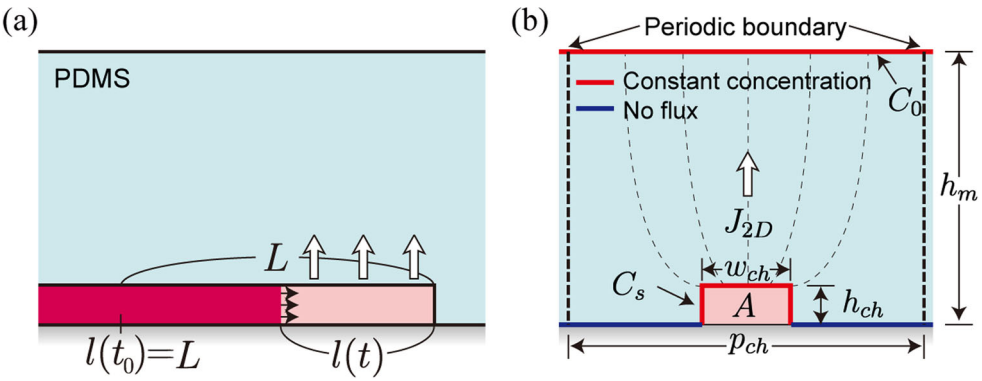

Fig. 3 Simulation model for the ink filling process. **a** The model of ink flow; **b** cross section of channel and boundary conditions of two-dimensional simulation of diffusion

Table 1 Comparison with 1D approximation and 2D simulation

1D approximation	Block ($h_m = 10$ mm)			Membrane($h_m = 0.45$ mm)		
$J_{1D,s}(w_{ch} + 2h_{ch}) \times 10^{-9}$	0.44			9.71		
$J_{1D,n}(w_{ch} + 2h_{ch})/\sqrt{t} \times 10^{-6}$	0.27			0.27		
FEM simulation	Block ($h_m = 10$ mm)			Membrane ($h_m = 0.45$ mm)		
Pattern density (w_{ch}/p_{ch})	10%	50%	91%	10%	50%	91%
$J_{2D,s} \times 10^{-9}$	4.33	0.87	0.48	82.34	19.56	10.80
$J_{2D,n}/\sqrt{t} \times 10^{-6}$	1.40	0.36	0.20	1.40	0.36	0.20

flux at the boundary in a steady and non-steady state are as follows:

$$J_{1D,s} = D\frac{C_s - C_0}{h_m} \tag{2}$$

$$J_{1D,n} = C_s\sqrt{\frac{D}{\pi t}} \tag{3}$$

where h_m is a thickness of the media of which a concentration at another side is C_0. Because non-steady solution describe the diffusion of semi-finite media whose initial concentration is zero, C_0 and h_m does not appear in Eq. 3. So, it is expected that when solvents are contacted with a template, the flux independent from the thickness of media happens at a boundary and gradually decreased until the one for steady states. The simplest approximation of J_{2D} is the integration of the boundary flux of the 1D model along the inner wall of the channel as follows:

$$J_{2D} \approx J_{1D}(w_{ch} + 2h_{ch}) \tag{4}$$

Note the approximation of Eq. 4 does not count a pattern density of channel because two-dimensional diffusion is truncated. For more accurate estimation of J_{2D} in which the pattern density is considered, FEM simulator (COMSOL Multiphysics) is used to obtain the flux of steady state ($J_{2D,s}$) and non-steady state ($J_{2D,n}$) with the periodic and two-dimensional models shown in Fig. 3b. The flux simulated in the time-dependent simulation is confirmed to obey the function of an inverse square root of time. Comparison between the analytical approximation and computational result and a list of parameters are summarized in Tables 1 and 2, respectively. This result shows the approximation using a peripheral length of channel matches with the simulation only when pattern density is high. It should be noted that the time until the template becomes a steady state can be roughly estimated by calculating the time the flux for non-steady state becomes smaller than the steady states. From the simulation results in Table 1, it is predicted that a 450-μm thick PDMS membrane will become steady condition within 5 min, while a 10-mm PDMS block takes 2460 min in any printing densities. As our printing time with PDMS block is much smaller than this value in general, the ordinal printing with the bulk template is most likely carried in a non-steady state of diffusion.

Now, solutions of the ink position to Eq. 1 can be found with the initial condition ($l_{s,n}(t_0) = L$) as follows:

$$l_s(t) = Le^{-K(t-t_0)}, \tag{5}$$

$$l_n(t) = Le^{-2K'(\sqrt{t}-\sqrt{t_0})}, \tag{6}$$

where K and K' are values independent of time expressed by the following:

$$K = J_{2D,s}\frac{1}{A}\frac{M_i}{\rho_i}, \tag{7}$$

Table 2 Parameters used in calculation and simulation ($T_p = 43.3\,^{\circ}C$)

Material properties			
D_P	Dffusion constant of PDMS (EtOH, 43.3 $^{\circ}C$)	1.88×10^{-10}	m^2s^{-1}
C_S	Saturation concentration of EtOH in PDMS	1170 [20]	$molm^{-3}$
C_0	Molar concentration on free boundary (EtOH)	8.0	$molm^{-3}$
ρ_i	Density of solvent (EtOH)	789	kgm^{-3}
M_i	Molar mass of solvent (EtOH)	46.07	$molg^{-1}$
Geometry parameters			
w_{ch}	Width of channel	20×10^{-6}	m
h_{ch}	Height of channel	5×10^{-6}	m
p_{ch}	Pitch of channel	200×10^{-6}	m
h_m	Thickness of template	10×10^{-3}	m
		0.45×10^{-3}	

$$K' = \frac{J_{2D,n}}{\sqrt{t}} \frac{1}{A} \frac{M_i}{\rho_i}. \quad (8)$$

Experimental verification of our prediction of printing speed is carried by observing actual ink filling in a block template. Figure 4 a is the result of l(t)with 10% pattern density ($w_{ch}/p_{ch} = 0.1$) and channel length (L) of 0.01 m. The stationary solution with $K = 2.53\times10^{-3}(\mathrm{s}^{-1})$ acquired by FEM does not match with the result, while the non-steady solution with simulated value of $K' = 0.82(\mathrm{s}^{-3/2})$ and $t_0 = 4300$ s is in good agreement with measured data ($\chi^2 = 0.29 \times 10^{-3}$). The t_0 is a reasonable value by considering a template cleaning with ethanol right between printings in addition to the pre-filling time. This result indicates that block membrane is partially saturated before the ink flow started at the observation point.

Thanks to the verified model of the template printing above, we can expect the printing speed of the block template and membrane template with various pattern densities. Ink flow speed is defined by dividing 95% of length by the time when $l(x,t)$ becomes 5% of total length. As shown in Fig. 4b, the ink flow speed will be improved by three to five times by altering block template with a 450-μm thick membrane. Please note that permeation speed can be improved further by using a thinner template if the diffusion is in a steady state according to the Eq. 2. The basis of some of the numbers in Table 2 is given here. First, the concentration of ethanol at the other side of a template (C_0) is obtained by the ideal gas law ($C_0 = P_e/(RT)$), where P_e is saturated vapor pressure of ethanol, and R is the ideal gas constant, 8.314 $\mathrm{m}^3 Pa K^{-1}$ mol^{-1}. The saturated vapor pressure of ethanol are calculated to be $21.28 \times 10^3 Pa (T_P = 43.4\,^\circ C)$ by the Antoine equation for ethanol [21], then $C_0 = 8.0$ $\mathrm{mol/m}^3$ is obtained. On the other hand, the diffusion constant at a specific temperature can be calculated according to the Stokes-Einstein equation. The diffusion constant in the printing temperature (T_P), D_P can be obtained as follows:

$$D_P = D_{RT} \frac{T_P + 273}{300} \frac{\mu_{RT}}{\mu_P}, \quad (9)$$

where μ_P and μ_{RT} are dynamic viscosity of ethanol in the printing temperature and room temperature. By calculating those viscosities from the study [22], the diffusion constant for the typical printing temperature ($43.4^\circ C$) is calculated to be $1.88 \times 10^{-10}\mathrm{m}^2\mathrm{s}^{-1}$. Here, the diffusion constant of PDMS for ethanol solvent is assumed to be $D_{RT} = 1.2 \times 10^{-10}$ according to various studies in a past [20, 23].

3 Pneumatic membrane printer

3.1 Printer head and printing system

Satisfying both of thinning of a template and uniform contact with the substrate are realized by using pneumatic action of a membrane. Figure 5 a illustrates a printer head which can inflate a membrane after contacting with a substrate. Some of the bolts fastening the membrane have a hole so that ink is supplied to the space between the substrate and the inflated membrane. The printer head has a space between the membrane and transparent lid on the other side where the dried gas flows with appropriate pressure.

Fabrication of membrane template is done by replicating Si master mold which has SU-8 (Microchem, Westborough, MA, USA) or TMMR (Tokyo Ohka Kogyo, Kanagawa, Japan) into PDMS film. PDMS film is made by spin coating of Sylgard184 mixed with a curing agent in 1:10 weight ratio. Uniform thickness ($\pm$ 10 μm) is achieved by multiple coating and rapid curing using a leveled hotplate (400 rpm spin coating and 100 $^\circ C$ hot plate for three times). When the aspect ratio of a template is high, removing the bubble

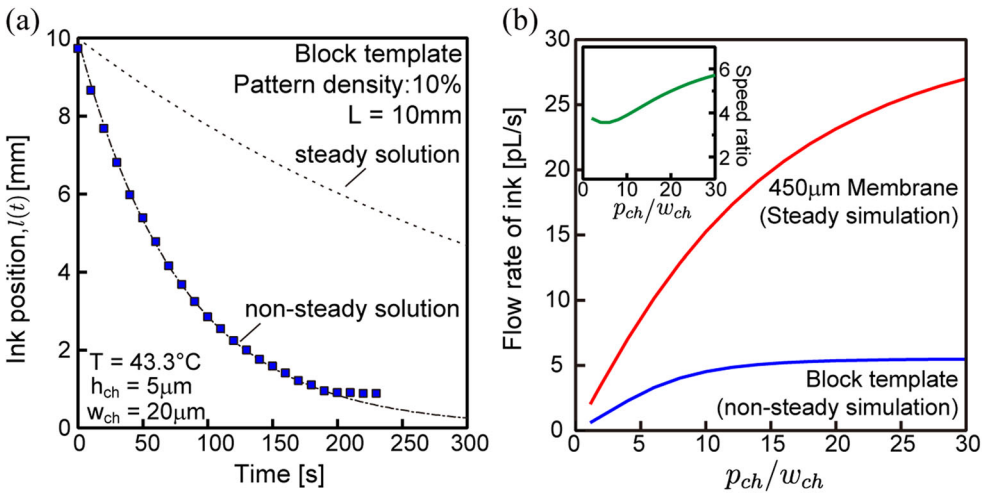

Fig. 4 Determination of parameters for the accurate prediction of printing speed. **a** Matching with experimental result with a block template, **b** expected improvement of printing speed

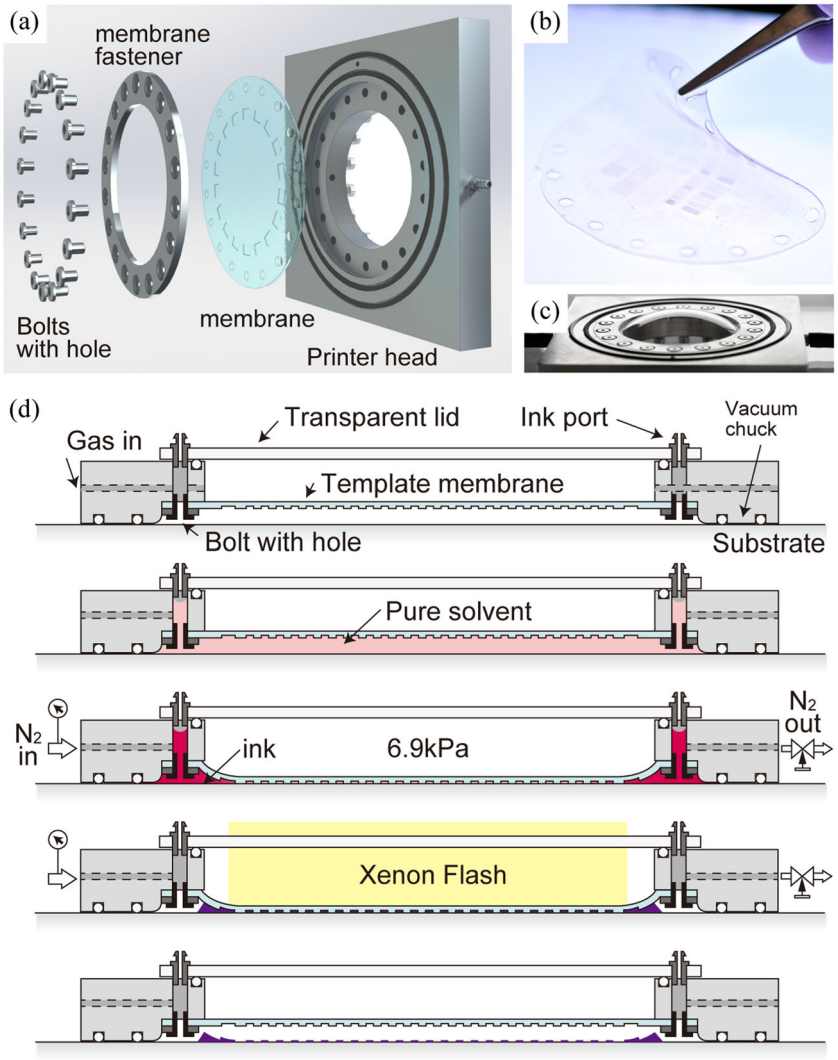

Fig. 5 Design of the printer head and printing procedure. **a** Assembly drawing of a printer head; **b** fabricated template membrane; **c** inflated membrane; **d** procedure of the printing

is necessary to maintain the membrane is durable enough to inflate. After the membrane is gently peeled from the master mold, a mounting of the membrane on to the printer head is carried in an ethanol tub to avoid initial stress or wrinkles. Figure 5 b and c show the fabricated membrane and inflated condition for reference.

Figure 5 d describes a procedure of the printing. After contacting and vacuum chucked with a substrate, the space between the membrane and substrate is filled with a pure solvent to initiate the permeation pumping. This solvent also works as a lubricant which enables deformation occurs only near the edge of a membrane. The nitrogen gas is introduced with the pressure of 6.9 kPa (1psi) which is smaller than the saturated vapor pressure of ethanol (20.9 kPa in T_P needle valve at an exhaust port controls the nitrogen gas flow about 100 sccm. Ink is then injected into space between the curved membrane and substrate through the holes of bolts. After most of the features are solidified, remaining ink on the reservoir is washed away and collected for regeneration by circulating ethanol while the template is pressed. If the printed material can be sintered by phone energy, flash sintering is then carried to avoid residue on template after release and increase adhesion for the following process. Releasing of the membrane is done by simply shutting a valve at the intake port. These procedures are done by manual gas control as shown in Fig. 6a. The printer head is fixed to an acrylic platen (Fig. 6b) and the printing is carried while temperature and pressure are monitored for better repeatability.

3.2 Demonstration of printing

In this section, the capability and feasibility of the membrane printer are presented visually. Figure 7 is sequence photographs taken through the transparent platen of the printer head while printing a conductive pattern with the EtOH-based silver nanoparticle ink, DGP 40LT-15C (ANP USA., Inc., Fremont, CA, USA). It can be seen that an ink

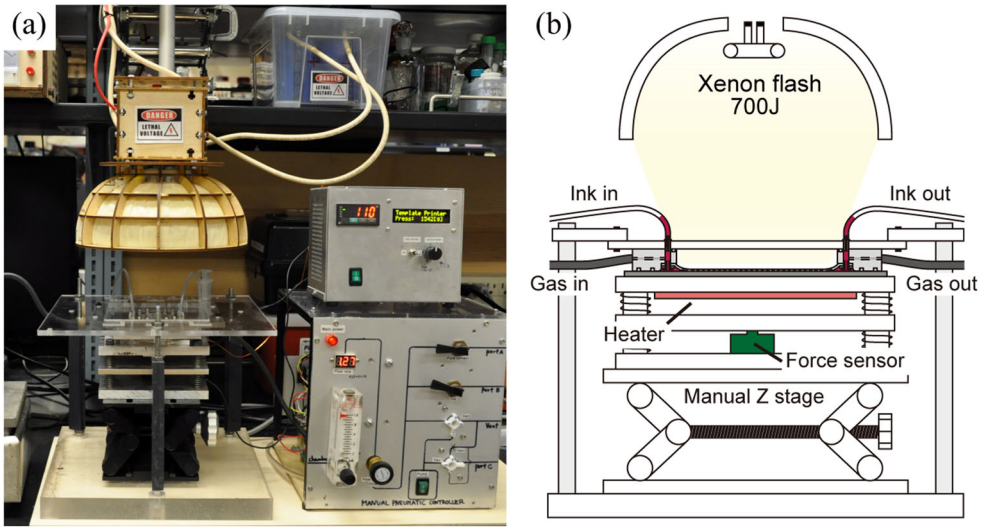

Fig. 6 Membrane printing system. **a** Photograph of the membrane printer. **b** Cross-sectional view of the core structure

reservoir is formed around the membrane and ink flows toward a center. As the concentration of ink builds up, the solidifying starts from the end of channels. Once the ink is injected to the reservoir, no additional operation is required, while the ordinal printing method needs supplying an ink or solvent constantly to prevent an ink reservoir dried in the middle of printing [24].

The sintering machine is integrated into this printer for several purposes. First is to increase the printing speed by skipping persistent heating before mold release which is used to be carried to prevent damage to the pattern [25]. The second purpose is to realize an in-situ cleaning of the substrate or mold before the printer head is released from the substrate. Figure 8 shows the demonstration of flash sintering on printed the silver pattern. The laboratory-made photon sintering machine can generate 420 mJ cm^{-2} of Xenon's flash within a few milliseconds. As shown in Fig. 8a, several times of an impulsive light exponentially decrease a sheet resistance of printed pattern which indicates the particles are sintered to some extent. The surface of the sintered pattern is observed by the scanning electron microscopy (SEM) to have larger and dense particles. The solvent resistance is also investigated by soaking into ethanol (Fig. 8c). The notable changes are

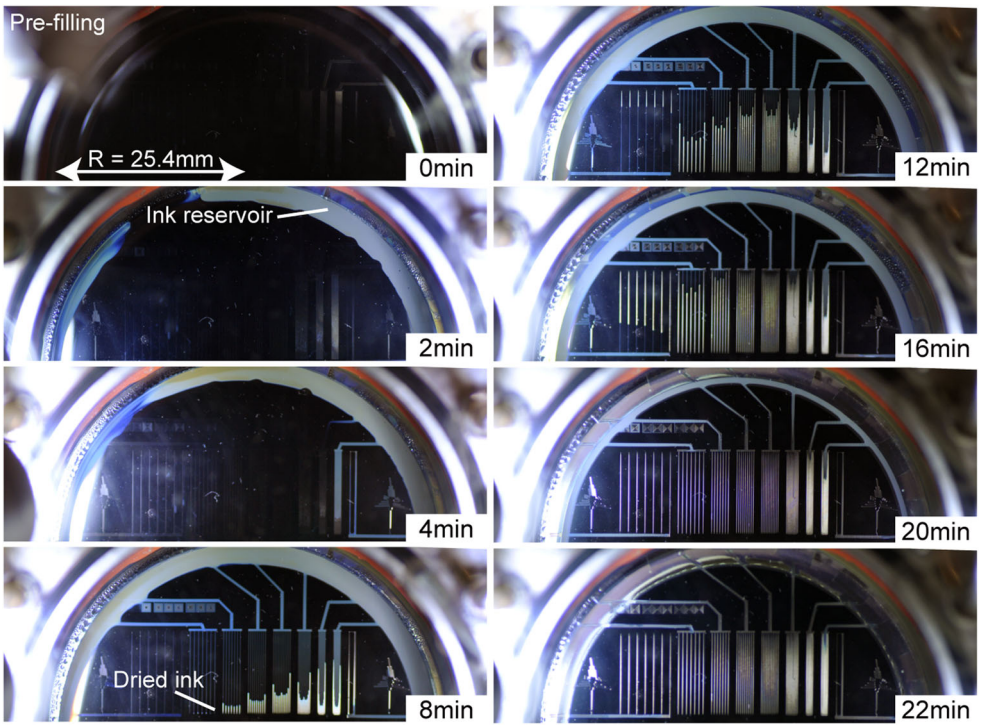

Fig. 7 Sequential photographs of the printer head while printing

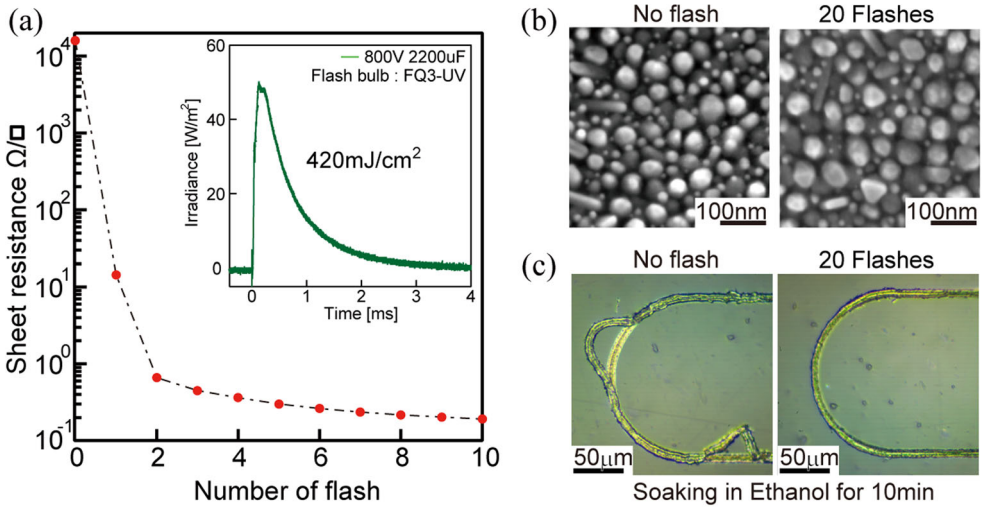

Fig. 8 Evaluation of sintering process. **a** Change of sheet resistance with number of flash; **b** SEM image of surface of printed pattern before and after flashing; **c** sintering effect on solvent resistance

observed which support feasibility of the in situ solvent cleaning after mold releasing.

The consistent procedure developed above realizes the high-throughput printing of complicated pattern shown in Fig. 9. These patterns are made of silver and printed by the template printing technology. Both of two patterns are printed within 20 min and no additional process is required. Figure 9 b is a demonstration of the printing uses a template with different height of microchannel.

4 Experiments and discussion

4.1 Ink filling of membrane template

First of all, the ink filling speed with a 450-μm thick template are investigated to confirm if the diffusion of thin PDMS membrane can be described as a steady state. Figure 10 shows the sequential photograph of the printing the pattern whose pattern density is 10%. As theoretically expected, the ink filling process becomes five times faster than that with a block template by altering it with a thin membrane. The analytical solution for the ink flow ($l(t)$) in a steady state well matches with the experimental result ($\chi^2 = 95.8 \times 10^{-6}$). The constant value, K of 4.81×10^{-2} calculated in Section 2.1 is used. This good agreement between experiment and simulation indicates that diffusion is the governing phenomena in this printing method and parameters in Table 2 are reliable.

Next, the investigation of ink flow rate and the drying rate of ink with different pattern densities are carried with both ordinal template and new membrane printer. The progress of printing with the template which has a test pattern with various densities is recorded by a camera, and printing speed is obtained by measuring the time when 95% of the channel is filled. As shown in Fig. 11a, the faster ink filling speed is observed which matches with the analytical simulation. By comparing the speed with block and membrane template, it can be concluded that the five times larger effective diffusion constant is realized by the new printer. On the other hand, drying speed is improved by a factor of two in average, which is not directly reflected by the change of diffusion constant (Fig. 11b, inset). This can be explained by considering an analytical model of the ink drying process.

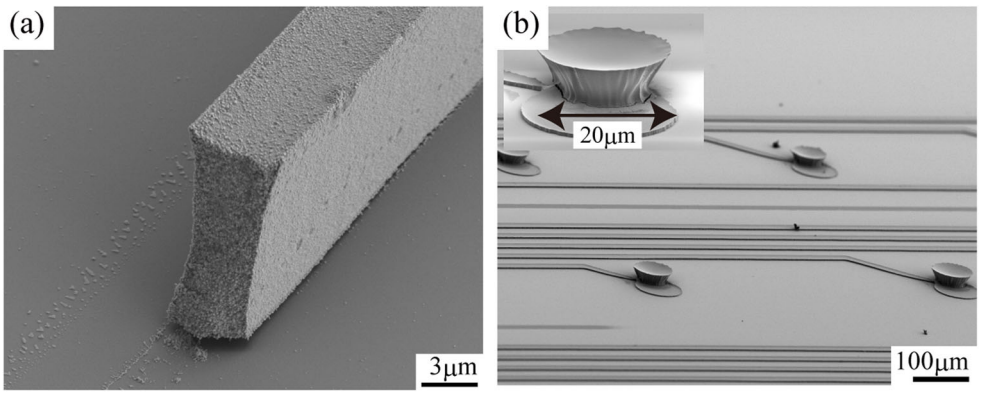

Fig. 9 Possible structure with the template printing technologies. **a** 5:1 aspect ratio structure **b** bump structures

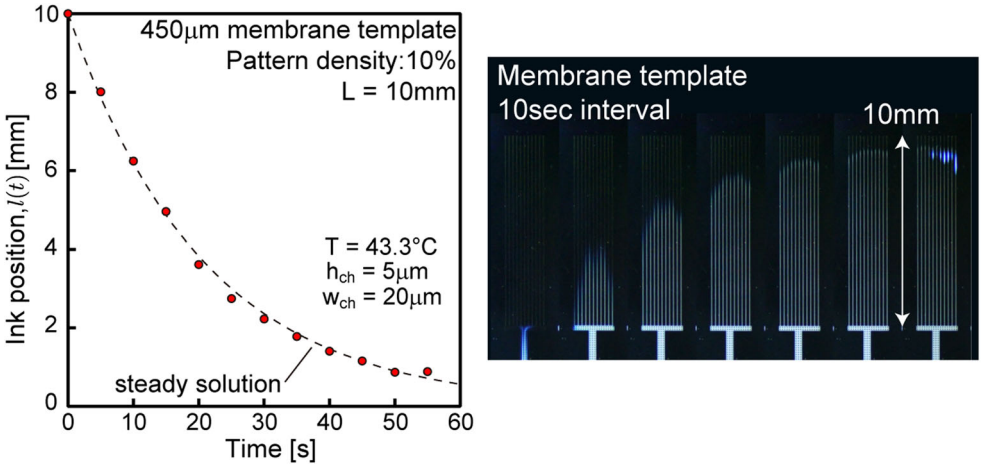

Fig. 10 Ink flow measurement in 450 um membrane template

The length of the undried channel can be expressed in the following equation [26] as follows:

$$l_{\text{dry}}(t) = L_p \exp\left(-\frac{C_0}{C_f} K(t - t_f)\right), \tag{10}$$

where L_p is the distance from an ink reservoir to the end of a channel and t_f is the time when solidarization started. The saturation concentration of ink C_f and the solute concentration of an ink reservoir C_0 appears as an additional time constant. We believe that the concentration of ink reservoir for block template is high compared to the membrane template because the block template printing uses an open-air ink reservoir as shown in Fig. 1a.

4.2 Other parameters affect the printing speed

The influence of other printing parameters on permeation speed is investigated here. Figure 12 a plots the ink filling speed with different printing temperature. The ratio between measured ink flow rates is 1.23 in average, and this is close to the ratio between diffusion constant in 43.3 °C (1.88×10^{-10}) and in 48.9 °C (2.11×10^{-10}) obtained from Eq. 9. As printing speed in steady diffusion is proportional to the value K ($L/t_f = KL/\log_e(0.05L)$) , this result is natural. Moreover, the increase of the speed regardless of the pattern density is a reasonable result as the diffusion constant is the parameter independent from geometry. Figure 12 b plots drying speeds with a different solute concentration of ink. The ink DGP 40LT-15C (metal content 31.6 wt%) is diluted with 200 proof ethanol at a specific rate. As Eq. 10 expected, a time constant of the drying process and an ink concentration must be in a proportional relation. The averaged ratio of printing speed is 2.8 which is close to the ratio of ink concentrations (19.0:6.3 wt%).

5 Summary

In this paper, a novel printing method using an inflatable template is proposed, and a comprehensive study from theory to experiments is carried to proof the feasibility of

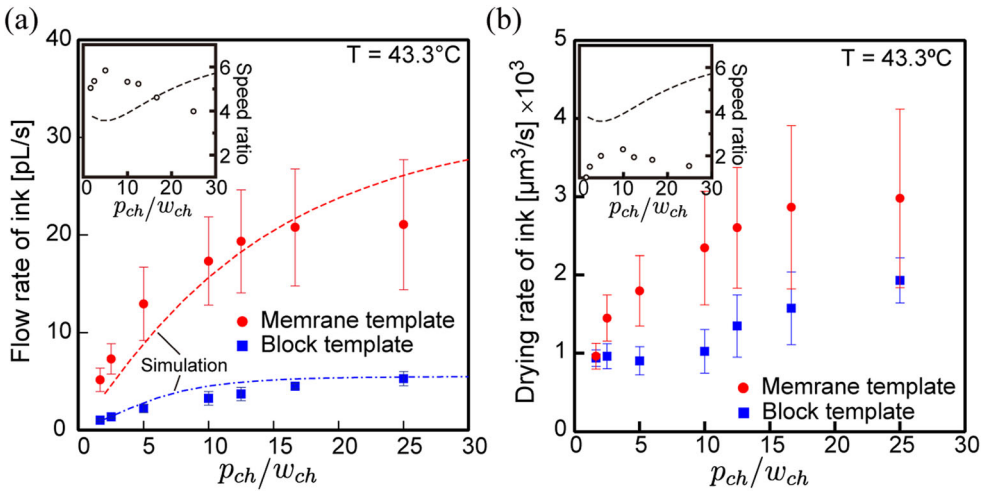

Fig. 11 Comparison between block and membrane templates: **a** ink filling rate and **b** drying rate of ink

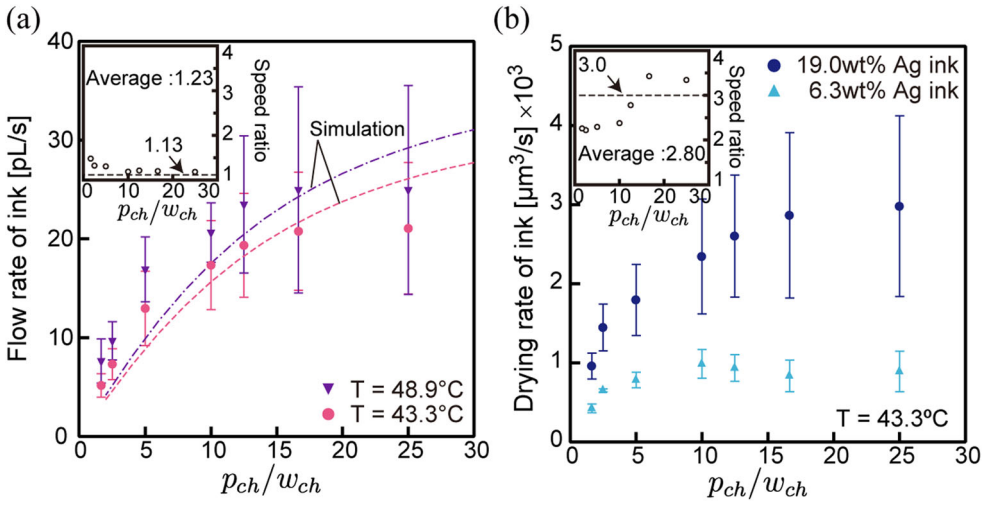

Fig. 12 Influence of other parameter on printing speed. **a** Permeation speed with different temperature; **b** ink concentration dependency on drying rate of ink

this method. Use of a membrane instead of a block has a benefit in printing speed and automation of a printing procedure. Diffusion analysis of templates reveals that 450-μm thick membrane has a constant permeation flux while the one for 10-mm thick template has a time-varying permeation speed which depends on the saturation condition of the block. The printer which can inflate the membrane, inject ink, and release the membrane after the ink dries is prototyped for reliable experimental proof of concept. The experiment shows that this method has a five times faster permeation rate than the ordinal method as expected. This degree of improvement is hard to achieve by increasing printing temperature or ink concentration. Moreover, micro-sized 3D structures are successfully demonstrated thanks to the semi-automated printer. In conclusion, the feasibility of printing method using an inflatable template is proven by numerical printing model and printing experiments, and this paper argued a new direction of research toward practical realization of a template printing technology.

References

1. Gates BD, Xu Q, Stewart M, Ryan D, Willson CG, Whitesides GM (2005) New approaches to nanofabrication: molding, printing, and other techniques. Chem Rev 105(4):1171–1196
2. Geissler M, Xia Y (2004) Patterning: principles and some new developments. Adv Mater 16(15):1249–1269
3. Khan S, Lorenzelli L, Dahiya RS (2015) Technologies for printing sensors and electronics over large flexible substrates: a review. IEEE Sens J 15(6):3164–3185
4. Saengchairat N, Tran T, Chua C-K (2017) A review: additive manufacturing for active electronic components. Virtual Phys Prototyp 12(1):31–46
5. Calvert P (2001) Inkjet printing for materials and devices. Chem Mater 13(10):3299–3305
6. de Gans B, Duineveld P, Schubert U (2004) Inkjet printing of polymers: state of the art and future developments. Adv Mater 16(3):203–213
7. Park J-U, Hardy M, Kang SJ, Barton K, Adair K, kishore Mukhopadhyay D, Lee CY, Strano MS, Alleyne AG, Georgiadis JG, Ferreira PM, Rogers JA (2007) High-resolution electrohydrodynamic jet printing. Nat. Mater. 6:782
8. Onses MS, Sutanto E, Ferreira PM, Alleyne AG, Rogers JA (2015) Mechanisms, capabilities, and applications of high resolution electrohydrodynamic jet printing. Small 11(34):4237–4266
9. Vaezi M, Seitz H, Yang S (2013) A review on 3D micro-additive manufacturing technologies. Int J Adv Manuf Technol 67(5):1721–1754
10. Wan AB, Kukjoo K, Heejoo L, So-Yun K, Yulhui S, Dae-Young L, Yeob SJ, Jang Ung P (2015) High-resolution printing of 3D structures using an electrohydrodynamic inkjet with multiple functional inks. Adv Mater 27(29):4322–4328
11. Gerber M, Beddingfield C, O'Connor S, Yoo M, Lee M, Kang D, Park S, Zwenger C, Darveaux R, Lanzone R, Park K (2011) Next generation fine pitch Cu Pillar technology - enabling next generation silicon nodes. In: 2011 IEEE 61st electronic components and technology conference (ECTC), pp 612–618
12. Orii Y, Toriyama K, Noma H, Oyama Y, Nishiwaki H, Ishida M, Nishio T, LaBianca NC, Feger C (2009) Ultrafine-pitch C2 flip chip interconnections with solder-capped Cu pillar bumps. In: 2009 59th electronic components and technology conference, pp 948–953
13. Moga KA, Bickford LR, Geil RD, Dunn SS, Pandya AA, Yapei W, Fain JH, Archuleta CF, O'Neill AT, DeSimone JM (2013) Rapidly–dissolvable microneedle patches via a highly scalable and reproducible soft lithography approach. Adv Mater 25(36):5060–5066
14. Kim Y-C, Park J-H, Prausnitz MR (2012) Microneedles for drug and vaccine delivery. Adv Drug Deliv Rev 64(14):1547–1568
15. Demko MT, Cheng JC, Pisano AP (2010) High-resolution direct patterning of gold nanoparticles by the ic molding process. Langmuir 26(22):16710–16714
16. Kim E, Xia Y, Whitesides GM (1995) Polymer microstructures formed by moulding in capillaries. Nature 376:581
17. Leng J, Lonetti B, Tabeling P, Joanicot M, Ajdari A (2006) Microevaporators for kinetic exploration of phase diagrams. Phys Rev Lett 96(8):84503
18. Moreau P, Dehmoune J, Salmon J-B, Leng J (2009) Microevaporators with accumulators for the screening of phase diagrams of aqueous solutions. Appl Phys Lett 95(3):33108
19. Randall GC, Doyle PS (2005) Permeation-driven flow in poly(dimethylsiloxane) ic devices. Proc Natl Acad Sci USA 102(31):10813. LP–10818

20. Duineveld PC, Lilja M, Johansson T, Inganäs O (2002) Diffusion of solvent in PDMS elastomer for micromolding in capillaries. Langmuir 18(24):9554–9559
21. Kretschmer CB, Wiebe R (1949) Liquid-vapor equilibrium of ethanol–toluene solutions. J Am Chem Soc 71(5):1793–1797
22. Mamedov AA, Aleskerov AM, Shikhaliev AY, Khalilov ShKh (1973) Variation of the viscosities and densities of carbon tetrachloride, ethanol, and their binary mixtures with temperature and concentrations, Viniti:1–8
23. Yi-Ming S, Jack C (2018) Sorption/desorption properties of ethanol, toluene, and xylene in poly(dimethylsiloxane) membranes. J Appl Polym Sci 51(10):1797–1804
24. Demko MT, Cheng JC, Pisano AP (2012) Rigid, vapor-permeable poly(4-methyl-2-pentyne) templates for high resolution patterning of nanoparticles and polymers. ACS Nano 6(8):6890–6896
25. Terasaki N, Dorsey K, Makihata M, Pisano AP (2017) Micro printing using microfluidics for printed biodegradable devices in trillion sensing. ECS Trans 75(41):13–19
26. Demko MT (2012) High resolution additive patterning of nanoparticles and polymers enabled by vapor permeable polymer templates, UC Berkeley, ProQuest ID Demko_berkeley_0028E_12305, Merritt ID: ark:/13030/m5125xk2. Retrieved from https://escholarship.org/uc/item/37n411xf